Nanoscale Advances

PAPER

View Article Online
View Journal | View Issue

Cite this: *Nanoscale Adv.*, 2023, 5, 4809

Received 8th May 2023
Accepted 26th July 2023

DOI: 10.1039/d3na00312d

rsc.li/nanoscale-advances

Time-resolved *in situ* nanoparticle size evolution during magnetron sputtering onto liquids†

Pinar Eneren, *[a] Anastasiya Sergievskaya, [b] Yunus Tansu Aksoy, [a] Polona Umek,[c] Stephanos Konstantinidis [b] and Maria Rosaria Vetrano[a]

Despite extensive research since 1996, there are still open questions regarding the primary location of the nucleation process, the growth mechanism of the nanoparticles (NPs), and the influence of the liquid properties on the ultimate size of the NPs for the magnetron sputtering of metals onto liquids. Hence, for the first time to the authors' knowledge, the particle size evolution is *in situ* and in real-time examined during and after the sputtering of the silver atoms onto silicone oil, *i.e.*, Sputtering onto Liquids (SoL) process. The particle size distribution (PSD) is measured *via* the Light Extinction Spectroscopy (LES) technique, and the deposition rate and stirring speed effects on the PSDs are analyzed. Based on De Brouckere mean diameters, the size evolution of silver nanoparticles (Ag NPs) over time is monitored. Ag NPs bigger than 20 nm are detected, and the PSDs are shown to be poly-disperse, which is also supported by the *ex situ* TEM measurements and *in situ* time-resolved absorption spectra. Moreover, it is shown that aggregation and growth of Ag NPs occur both at the plasma–liquid interface and inside the silicone oil during and after the magnetron sputtering. Despite the same amount of deposited silver, the growth kinetics of Ag NPs in silicone oil vary at different deposition rates. In particular, at higher deposition rates, larger NPs are formed. Stirring is seen to help disaggregate the particle lumps. Faster stirring does not substantially influence the final size but promotes the formation of smaller NPs (<20 nm). Also, low colloidal stability of Ag NPs in silicone oil is observed.

1 Introduction

There exist critical length scales below which materials' physico-chemical properties significantly differ: particles with diameters < 100 nm possess features unlike those of bulk solids.[1] These features of nanoparticles (NPs) are determined by their composition, size, size distribution, shape, and level of aggregation.[2] Owing to their superior characteristics (*e.g.*, thermal, electrical, and mechanical), NP synthesis attracts growing attention in various fields, such as material science, pharmaceutics, and biochemistry.[3–5] However, NP synthesis is susceptible to slight changes in experimental conditions (impurities in chemicals, dust, room temperature, humidity level, *etc.*), especially for large-scale production. It is therefore crucial to control those properties to tailor the NP characteristics for the foreseen applications.

NPs can be synthesized with physical, chemical, or physico-chemical methods.[6] In contrast to chemical synthesis that demands reducing and stabilizing agents, ultra-pure and well-dispersed nanofluids (colloidal mixture of base liquid and solid particles with at least one dimension <100 nm (ref. 7)) can be obtained without the formation of byproducts *via* physical syntheses,[8] *e.g.*, thermal evaporation, laser ablation, and sputtering, *etc.* In this respect, plasma-based magnetron sputtering of metals onto low-vapor pressure liquids is considered a green solution to the reproducibility and purity issues since they take place in a controlled environment, *i.e.*, in a vacuum chamber filled with inert gas.[9] During magnetron sputtering, metal atoms that first deposit onto the liquid surface later diffuse throughout the liquid. This mechanism differs from the classic wet-chemical synthesis, in which the NPs are supposed to be homogeneously formed inside the liquid. As a result, the composition and size distribution of NPs can be tailored through the working gas pressure, sputtering power (discharge voltage/current), sputtering duration, viscosity, and temperature of the host liquid, *etc.*[6]

The ionized inert gas atoms, such as Ar^+, bombard the target surface, provoking the physical ejection, *i.e.*, the sputtering phenomenon, of metal atoms and/or small primary clusters. However, no collisions among the sputtered species are expected in the gas phase at low pressures,[10] which is elucidated

---

[a] KU Leuven, Department of Mechanical Engineering, Division of Applied Mechanics and Energy Conversion (TME), B-3001 Leuven, Belgium. E-mail: pinar.eneren@kuleuven.be

[b] University of Mons, Plasma-Surface Interaction Chemistry (ChIPS), CIRMAP, Research Institute for Materials Science and Engineering, B-7000 Mons, Belgium

[c] Jožef Stefan Institute, Department of Condensed Matter Physics, Ljubljana, Slovenia

† Electronic supplementary information (ESI) available. See DOI: https://doi.org/10.1039/d3na00312d

as a straight path from the target to the substrate.[11] More in detail, the sputtered species preserve their initial kinetic energy in the absence of gas-phase collisions, and they do not scatter around. The metal influx exponentially decreases for increased gas pressure at a fixed sputtering power.[12,13]

Unlike the wet-chemistry synthesis where stabilizing agents are present, the growth rate of NPs in magnetron sputtering is restricted by the diffusion and coalescence rates of the NPs within the liquid.[9] In general, three particle growth situations are postulated: collision and growth of particles occurring only on the plasma–liquid interface,[14] inside the bulk liquid,[15,16] or in both.[10,17] The coordination of a volatile stabilizer with the sputtered species in the gas phase during the sputtering can suppress the coalescence of NPs during the nucleation stage in the liquid phase.[18]

As NPs have a high surface-to-volume ratio, they are prone to collide and coalesce to lower their total surface energy.[19] The growth, aggregation, and colloidal stability of NPs during and after the Sputtering onto Liquids (SoL) process highly depend on the selected sputtered metal[10] and the surface coordination ability of the bulk liquid's molecules.[14] Therefore, a host liquid having compatible surface coordination ability with the surface of the NPs can hamper the aggregation and aid the synthesis of size-controlled NPs.[20] Noteworthy, each host liquid exhibits particular stabilization capabilities for different NPs due to various chemical interactions between the liquid's molecules and the sputtered metals. For example, Au sputtering onto castor oil and polymerized rapeseed oil (chemically different vegetable oils with similar viscosity values) produces a well-dispersed nanofluid and a transparent film under identical sputtering conditions, respectively.[21] In the case of ionic liquids (ILs), the coalescence continues until metal NPs are stabilized by the adsorption of ILs' constituent ions acting as capping agents.[20] Modified collision/coalescence kinetics of the NPs during the thermal annealing results in larger particles both in spherical and anisotropic shapes.[19]

The temperature and viscosity of the host liquid are articulated to be influential also in the NP growth kinetics. Heating on the substrate is anticipated during deposition, mainly due to the high kinetic energy of the sputtered species.[22] As one of the major contributors to the consequent temperature gradient in the liquid (several tens of mW cm^{-2} energy flux density on the surface[23]), these sputtered species modify the growth and transport phenomena of the NPs. Indeed, thermocouple reading in the liquid is reported to be increasing during magnetron sputtering.[24,25] This temperature rise diminishes both the viscosity and surface tension of the liquid, leading to easy penetration of the sputtered species through the liquid surface.[9] The higher the liquid temperature, the higher the number of collisions among these species beneath the liquid surface, which may result in larger NPs,[18] *e.g.*, Au NPs in the ionic liquid 1-butyl-3-methylimidazolium tetrafluoroborate (C_4mim^+/BF_4^-)[14] and polyethylene glycol.[26] Apart from that, due to the high viscosity of the liquid, a thin film can be created on the substrate.[21,24,27,28] Metal atoms do not have sufficient time to diffuse through it, favoring lateral growth. The higher the liquid viscosity, the slower the nanoparticle growth[29] and the transport of the NPs, which may end up with bigger NPs.[16,21,28] This can be beneficial for the coating of ILs with a highly reflective metal surface to serve as a lunar liquid mirror telescope.[30]

The metal influx is reported to have a linear relation with respect to the increased sputtering power at a fixed gas pressure. Besides, bigger NPs may be obtained at a higher discharge voltage, corresponding to the higher kinetic energy and enhanced diffusivity of the sputtered species.[31,32] This might be related to different heating levels on the liquid surface since no size change for the NPs is also reported.[11,15] A darker-colored nanofluid is expected after a longer sputtering experiment due to the higher particle concentration.[33] Ambiguity exists for the effect of longer sputtering on the size of the NPs. Some researchers claim no impact and only the increase in particle concentration,[11,15,18,20,31,34] while some argue that as a consequence of the increased particle concentration, collision frequency among the sputtered species and NPs is promoted, causing larger NPs to form.[10]

Current magnetron sputtering measurements lack *in situ* and real-time particle size characterization. In other words, the nanofluids must be sampled and even partially treated or diluted after the SoL experiments for several posteriori analyses. Nonetheless, sampling may introduce uncertainties and involve inevitable human errors, leading to inconsistencies among the experimental results.[35] In addition, the granular state of the nanofluids may change due to sampling.[36] Further, there might be very long time laps between the production of NPs and the time they are characterized. The Light Extinction Spectroscopy (LES) technique, on the other hand, does not require any sampling and can be applied to a broad particle size range (a few tens of nm to a few microns). Owing to its non-intrusiveness, the interactions at the plasma–liquid interface and the NP growth mechanism are unperturbed.

In this research, the particle size evolution of magnetron sputtering of the silver atoms onto silicone oil is *in situ* and real-time examined for the first time. The experiments are performed using a Direct Current Magnetron Sputtering (DC-MS) power supply to ignite the plasma inside a vacuum chamber at low Argon gas pressure of 0.07 Pa. The effects of the sputtering power and the duration of the plasma treatment on the particle size distribution (PSD) are investigated, as well as the rotational speed of the stirring bar for the mixing.

2 Materials & methods

2.1 LES technique

The LES technique focuses on the transmittance of a collimated poly-chromatic light beam passing through a medium populated with an ensemble of particles (see Fig. 1) and allows

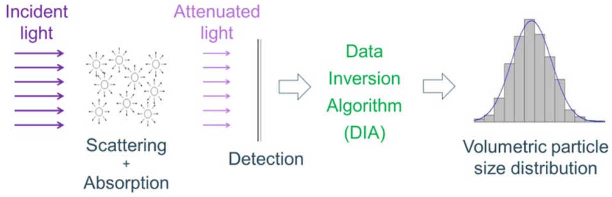

Fig. 1 The principle of the LES technique: light intensity attenuates due to particles/droplets.

determining their size distribution. Owing to the incorporation of broad light spectra, *a priori* shape information of the PSDs is no longer required. The light intensity of the beam attenuates due to the scattering and absorption characteristics of the particles, and their sum is called extinction. The spectral components of the attenuated light depend on its wavelength, the relative complex refractive index spectrum of the particles to the medium, and the size, shape, and concentration of the particles.[37] The light extinction can be analytically modeled by the Lorenz–Mie theory[38] that solves the scattering of a plane electromagnetic wave by a spherical, homogeneous, non-magnetic, and non-porous particle, *i.e.*, *Mie scatterer*. Owing to its simplicity, the Lorenz–Mie theory is still extensively applied for the calculation of the extinction cross-sections of nano-aggregates.[35] Then, the PSD in volume can be retrieved using an appropriate data inversion algorithm.

The resolution limit of the other optical methods (laser diffraction, dynamic light scattering, *etc.*) is dictated only by the scattering properties of the particles at a single wavelength. On the contrary, the LES technique involves both scattering and absorption characteristics of the particles over a broad wavelength range.[39] However, a clear parameter range, in terms of particle size and concentration, with a specific accuracy is quite compelling to be defined for the LES technique. Indeed, the optical properties of the particulate system, the signal-to-noise ratio of the experiment, the optical path length, the selected light scattering model, and the stability of the inversion algorithm play a significant role.[40] Moreover, inversion stability is mostly influenced by the signal quality of the measured transmittance and the accuracy with which the complex relative refractive index is known.[41] More details on the LES technique can be found in ref. 42 and 43 and some mathematical formulations are presented in the ESI.†

2.2 Experimental setup

The experimental setup consists of two parts: a deposition chamber for the SoL experiments and an optical assembly for the LES measurements. The schematic of the experimental setup is given in Fig. 2. Sputtering experiments take place in a cylindrical stainless-steel deposition chamber. A negatively-biased magnetron cathode holds a silver target, possessing a diameter of 5.08 cm, a thickness of 0.635 cm, and a purity of 99.99%. To meet stable deposition conditions, the cathode is water-cooled. The host liquid is low-vapor pressure, transparent, and chemically inert, *e.g.*, a silicone oil polydimethylsiloxane (PDMS, Sigma Aldrich, CAS number 63148-62-9) with the viscosity and surface tension of 50 cSt and 20.7 mN m^{-1}, respectively. No stabilizing agent is added to the silicone oil (6.8 g). The deposition occurs inside a quartz cuvette and the distance between the target and the liquid surface is 9.8 cm. The cuvette is fixed inside a holder on the transfer arm that can move through the load-lock and the main deposition chambers. A magnetic stirrer is placed beneath the cuvette so that the rotational speed of the stirring bar can be remotely regulated. To eliminate the water content, the silicone oil is first degassed in the load-lock chamber that is pumped down to 10^{-4} Pa. High-purity argon is injected into the deposition chamber at a constant flow rate of 30 sccm (standard cubic centimeter per minute) to generate the plasma. The surface of the silver target is then sputter-cleaned in the argon plasma prior to sputtering experiments. When the surface chemistry of the target is stabilized, the plasma is switched off, and then the cuvette is transferred from the load-lock chamber to the main deposition chamber. Finally, the plasma is reactivated for the desired amount of time at the desired sputtering conditions. During these experiments, a DC-MS power supply is used and the argon pressure is maintained constant at 0.07 Pa. The LES part is composed of emission and receiving optics. The former comprises a highly stabilized light source (DH-2000-DUV, Ocean Optics), two solarization-resistant optical fibers, an inline intensity attenuator, and a UV-VIS collimating lens. The receiving optics include a similar UV-VIS collimating lens, a solarization-resistant optical fiber, and a spectrometer (Maya2000-PRO, Ocean Optics) that is quite sensitive in the UV range (very high signal-to-noise ratio). Optical access is allocated in the vacuum chamber for the optical fibers, facing each other *via* vacuum feed-through accessories. Furthermore, fiber optics are rigidly fixed to a platform that can be moved up and down so that the LES measurements can be accomplished at different heights along the cuvette. The reference and attenuated light intensity data are recorded by the spectrometer with an integration time of 10 ms and transferred to a laptop to execute the data inversion algorithm required for the LES technique. The collimated light beam passes through the quartz cuvette having an optical path length of 2 cm and is located 1 mm below the plasma–liquid interface.

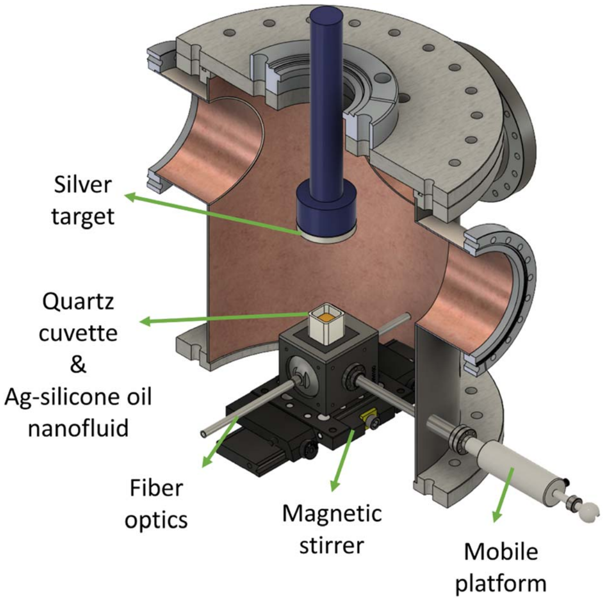

Fig. 2 Schematic of the setup. The main vacuum chamber is constructed to enable the LES measurements during magnetron sputtering experiments so that the PSDs of Ag NPs are *in situ* and in real-time characterized.

Table 1 Test matrix at total sputtering energy of 3 kJ and Ar pressure of 0.07 Pa. The distance between the silver target and the surface of the silicone oil is 9.8 cm

Test #	Applied power [W]	Sputtering time [min]	Stirring speed [rpm]
1	10	5	200
2	10	5	200
3	10	5	200
4	50	1	200
5	25	2	200
6	10	5	600

2.3 Conditions & test matrix

We investigate the effect of the applied sputtering power and sputtering duration, and the rotational speed of the stirring bar on the PSDs of Ag-silicone oil nanofluids. The sputtering power and the sputtering duration are varied in such a way that the total sputtering energy delivered to the silver target is kept constant (see test matrix in Table 1). In other words, the sputtering duration is lowered to compensate for the increasing silver influx, which is resultant of the increased sputter power. Due to the various heat sources (*e.g.*, plasma-born species, sputtered metal particles, plasma radiations, and the heated target), the temperature of the substrate may increase.[44] This increase would become substantial for the conditions where high sputtering power is applied for long durations.[15] Nonetheless, no significant temperature variation on the surface of the silicone oil is predicted in this work owing to the reduced sputtering duration for the tests with higher sputtering power. More specifically, the overestimated rate of the temperature rise on the liquid surface is 1 °C min^{-1} according to authors' recent study.[25] Hence, both ambient and nanofluid temperatures are expected to be around 24 ± 2 °C.

3 Results & discussions

Stabilization of Ag NPs can be difficult as the instabilities may originate from the surface oxidation or random aggregation.[45–47] Due to the plasmonic properties of Ag NPs,[48] the outcome of the magnetron sputtering can be detected even by the naked eye. An example of a successful deposition experiment can be seen in Fig. 3, in which Ag NPs are well-dispersed within silicone oil without any brown cloud-like spots, *i.e.*, no concentration gradient. Mixing *via* a stirring bar helps not only to prevent the temperature gradient during the deposition process but also to disperse the NPs within the liquid. In the absence of stirring, the particles would disperse only *via* diffusion, which would take more time. Plus, no particle sedimentation is anticipated owing to the constant stirring in the cuvette.

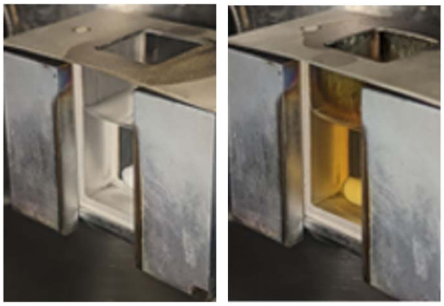

Fig. 3 Silicone oil in a quartz cuvette before (left) and after (right) the silver deposition. The stirring bar at the bottom helps enhance the particle dispersion.

3.1 TEM imaging

The size, shape, and composition of Ag NPs are determined *via ex situ* Transmission Electron Microscopy (TEM). TEM imaging is performed using a Jeol 2100 microscope operating at 200 kV. Four drops of Ag-silicone oil nanofluid are diluted with 3 mL of ethyl acetate. Two drops of the prepared dispersion are then deposited on a lacy carbon film supported by a copper grid (300 mesh) and dried on a hot plate at 50 °C. Thereafter, the grid is soaked in ethyl acetate for 5 hours and dried in air. Prior to TEM imaging, all samples are stored at room temperature and in the dark to minimize photo-induced oxidation. The acquired images are presented in Fig. 4 and analyzed with Digital-Micrograph software. The TEM results reveal the presence of spherical NPs with diameters ranging from 2 to 40–50 nm. The rings of the SEAD pattern of Ag NPs are assigned to (111), (200), (220), (311), and (331) lattice planes of face-centered cubic Ag (ICDD car. No. 04 0783) and indicate the polycrystalline nature of Ag NPs.

3.2 LES diagnostics

The scattering characteristics of the Ag NPs are considered to lie between the Rayleigh scattering regime (for small NPs) and the lower bound of the Mie scattering regime (for large particles).[49] If the particle cloud consists of small and randomly oriented particles, the LES technique becomes less sensitive to the particle morphology as opposed to the particles with high aspect ratio.[40] That is, the light extinction property is more sensitive to the size of the aggregates than their morphology.[35] It should be noted for the poly-disperse distributions that the scattering of larger particles can suppress that of smaller ones, depending on the size parameter.[50] During the LES measurements, Ag NPs are not subject to oxidation in the plasma owing to the lack of three-body collisions[16] under good vacuum conditions, and the NPs are composed of pure silver crystallites. Hence, for the LES diagnostics, the complex refractive index spectrum of pure bulk silver is extracted from ref. 51. The real part of the refractive index of the silicone oil is measured *via* the ellipsometry technique (Accurion EP3-SE Imaging Ellipsometer).

3.2.1 Absorption spectra & repeatability. One of the first *in situ* and real-time assessments on the nucleation and growth of Au NPs occurs through the chemical reduction process by using synchrotron SAXS/WAXS, and UV-VIS spectroscopy.[52] The temporal evolution of not only the UV absorption but also the PSD and number concentration helps to interpret the different stages of the growth kinetics. Likewise, Fig. 5 depicts the *in situ* and real-time absorption spectra of the Ag NPs in silicone oil during magnetron sputtering. While the plasma is on, the

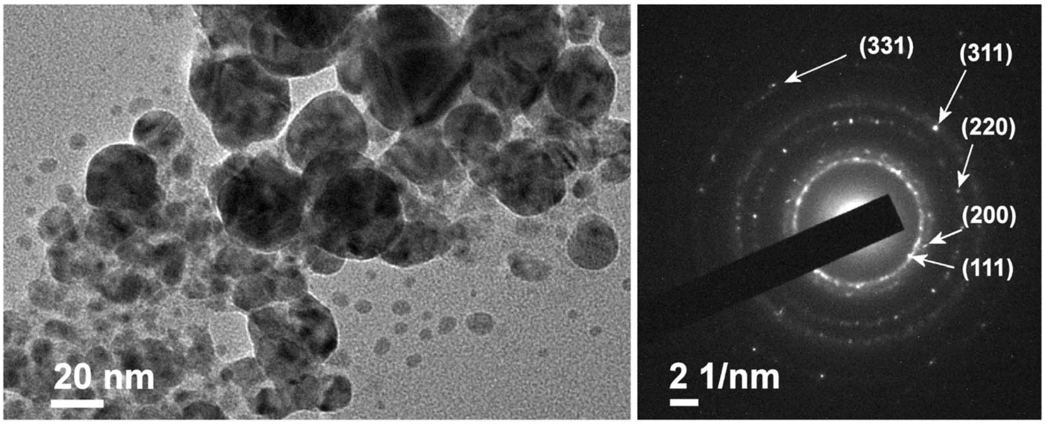

Fig. 4 TEM image of Ag NPs (left) and corresponding Selected Area Electron Diffraction (SAED) pattern (right) from Test 3. The SEAD pattern is showing the (111), (200), (220), (311), and (331) reflections of silver (ICDD car. no. 04 0783).

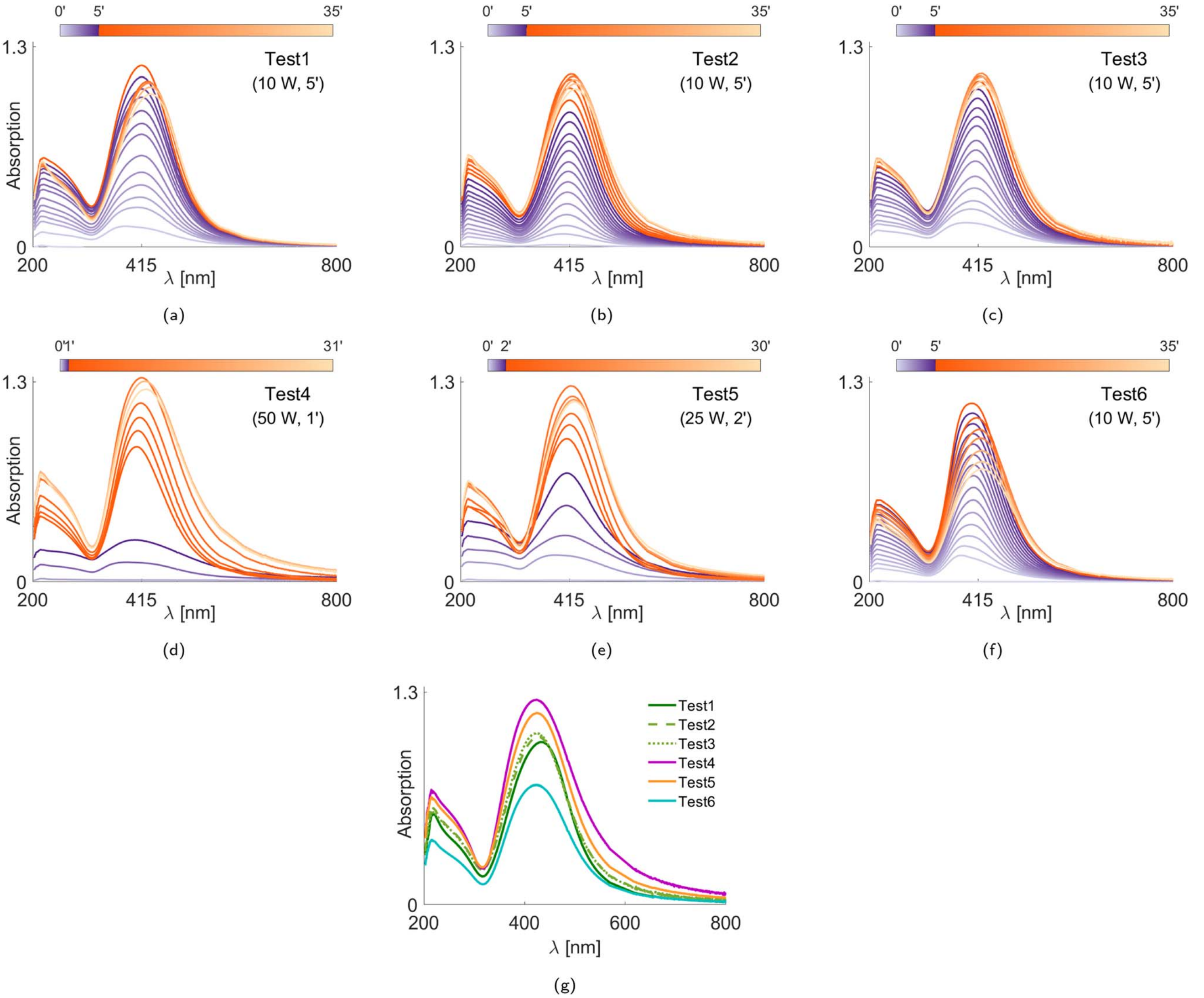

Fig. 5 *In situ* and real-time recorded absorption spectra of the Ag NPs in silicone oil (a–f) for Tests 1–6, respectively, and their comparison at the final acquisition, *i.e.*, ~30 minutes after the plasma is turned off (g). The violet curves express the temporal measurements when the plasma is on, whereas the orange curves show the temporal measurements after the plasma is turned off. The data acquisition rates are not identical.

absorption level rapidly increases, arising from the continuous silver influx and incorporation of Ag atoms in silicone oil (curves in violet color). Along the deposition period, the characteristic localized Surface Plasmon Resonance (SPR) bands emerge over time with the peak located around $\lambda = 410$–415 nm and remain invariant. Similar *in situ* absorption curves (peak around $\lambda = 410$ nm) are obtained during the chemical synthesis and growth of Ag NPs.[53] When the plasma is turned off, the absorption level starts to first increase (curves in orange color, reaching the maximum). This can be explained by an offset/delay in the detection time due to the presence of tiny particles (<3−4 nm) that cannot be detected in the absorption spectrum until they reach sufficient size. Afterward, the absorption level around the SPR peak decreases gradually, and the peak shifts towards longer wavelengths (red-shifting). Generally speaking, this tendency implies a broader PSD and/or particle aggregation.[40,54] The number of acquired data is lower in Tests 4 and 5 (lower number of violet curves) due to the shorter sputtering duration, *i.e.*, 1 and 2 minutes instead of 5 minutes. Test 6 exhibits unlike behavior to Tests 1–3 with a larger red-shifting in the SPR band due to higher stirring speed. In Fig. 5g, the latest absorption curves from Fig. 5a–f are plotted, which correspond to the acquisitions ∼30 minutes after the plasma is turned off. The resemblance in the absorption spectra among Tests 1–3 proves that the SoL experiments are well repeatable under similar conditions. Despite constant total sputtering energy and thus the same amount of deposited silver atoms, both the smaller peak at shorter wavelengths and the SPR bands deviate drastically under different deposition rates or stirring speeds. The evolution of the aforementioned characteristic Ag SPR bands is ascribed to the presence of metallic Ag NPs larger than 3–4 nm in diameter.[17,55] In fact, the absorption spectra in Fig. 5 display not only the growth of larger Ag NPs but also the formation of new small Ag NPs[56] (peak evolution at shorter wavelengths) from the aggregation of non-crystalline particles (<3−4 nm), for which the plasmon

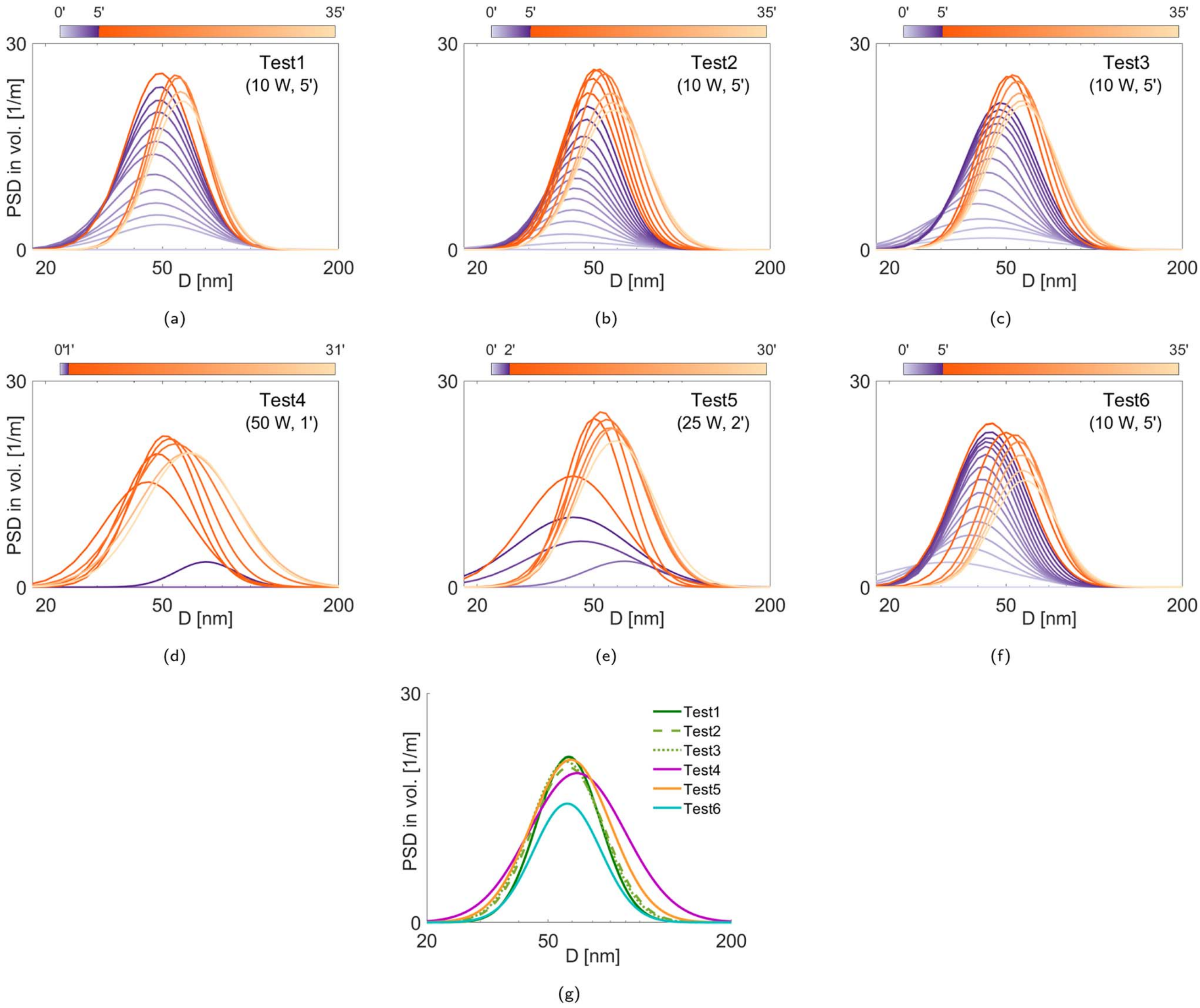

(a) (b) (c)

(d) (e) (f)

(g)

Fig. 6 *In situ* and real-time PSDs of Ag NPs in silicone oil (a–f), their comparison at the final acquisition, *i.e.*, ∼30 minutes after the plasma is turned off (g). The plasma is on (violet) and off (orange).

absorption is not observable,[17] and absorption depends only on the total metal concentration.[53] These very small primary clusters with low structural order grow *via* collisions and coalescence and form crystalline Ag NPs. Consequently, a bimodal[8,32,57,58] and poly-disperse PSD would be expected due to the coexistence of very small and relatively large Ag NPs since fresh nucleation and ongoing nanocrystal growth processes simultaneously happen during the deposition period.[24,59]

3.2.2 Particle size distributions. Fig. 6a–f present the temporal evolution of the PSDs of the population found *via* the LES technique, fitted with the assumption of log-normal distribution.[32,60,61] Since the LES technique cannot detect the tiny primary clusters without plasmon characteristics, the first detected Ag NPs in silicone oil have a diameter of $\sim$20 nm and we observe that Ag NPs continue to grow in silicone oil after the plasma is turned off (curves in orange color shifting towards larger diameters). Similar post-sputtering growth is also reported in the literature.[9,29,34,62,63] Nevertheless, this is the first *in situ* and real-time examination of the impact of the stirring speed on the PSD during SoL experiments to the best of the authors' knowledge.

Fig. 6g shows the PSDs obtained from the final acquisitions ($\sim$30 minutes after the plasma treatment). We see that the Ag NPs produced during Tests 1–3 are similar, demonstrating good repeatability of the measurements. We also see that, although the mode diameters do not strongly vary, the poly-dispersity of the PSDs depends on the selected experimental conditions. In particular, Test 4 yields the most poly-disperse PSD that includes the largest NPs, *i.e.*, it seems that the particles tend to aggregate more during faster deposition. To better understand the size evolution of the Ag NPs over time, we evaluate the volume mean diameter D_{43} (De Brouckere mean) for all test cases, as illustrated in Fig. 7, and the PSD properties corresponding to the final acquisition are listed in Table 2, including the Coefficient of Variation (CoV, dispersity level) of the particle population. In Fig. 7, we observe that slower deposition rates facilitate the formation of smaller NPs (Tests 1–3 and Test 6). On the contrary, larger D_{43} diameters (both initially and ultimately) are obtained at higher deposition rates despite the same amount of deposited silver. This can be due to an initial accumulation and clustering of particles already at the plasma–liquid interface and its vicinity before penetrating into the liquid.[64] These weak but bigger aggregates coming from the plasma–liquid interface disaggregate thanks to stirring, with a consequent increase in the population of smaller NPs, *i.e.*, a decrease in D_{43} diameters. Later, we observe an increase in D_{43} diameters, which should be due to the increased particle concentration, during which the aggregation is triggered. These aggregates cannot be disaggregated by stirring anymore, which is more evident in Tests 4 and 5. In other words, the temporal evolutions of D_{43} diameters exhibit a valley except for Test 6, which can be attributed to better mixing at higher stirring speed (200 rpm for Tests 1–5 *vs.* 600 rpm for Test 6). Despite the same silver deposition rates and similar ultimate D_{43} and CoV values shown in Table 2, Test 6 possesses a smaller peak value of the PSD in volume (*y*-axis in Fig. 6g) with respect to Tests 1–3. This means that compared to Tests 1–3, there are more particles smaller than the detection limit of the LES technique (<20 nm) in Test 6 to satisfy the conservation of mass. This confirms a certain limitation of aggregation with the increased stirring speed. A higher stirring rate is reported to enhance the diffusion both on the liquid surface and inside the liquid bulk, which hinders the NPs accumulation on the liquid surface and results in smaller NPs.[10,65]

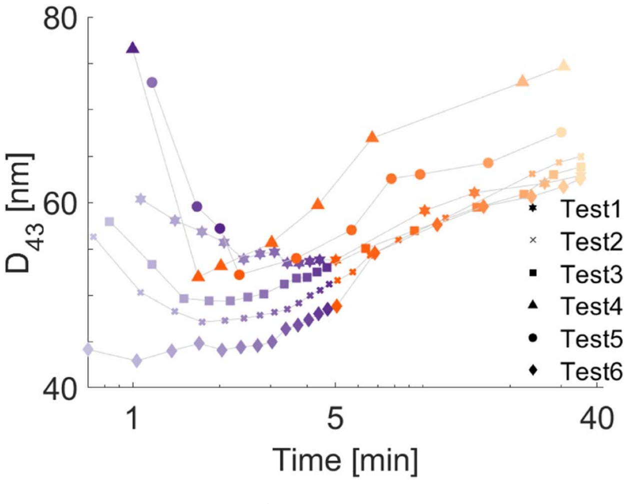

Fig. 7 Temporal evolution of D_{43} diameters with the uncertainty of ±1 nm.

Table 2 The properties of the final PSDs from Fig. 6g. D_{43} designates the volume mean diameter (De Brouckere mean) and CoV symbolizes the Coefficient of Variation (dispersity level) of the population

Test #	D_{43} [nm]	CoV [—]
1	62.8	0.24
2	64.9	0.27
3	63.8	0.27
4	74.6	0.37
5	67.5	0.30
6	62.5	0.25

4 Conclusions and perspectives

In this work, for the first time, *in situ* and real-time characterization of the particle size distribution (PSD) both during and after magnetron sputtering of the silver onto silicone oil experiments at low Ar gas pressure with a DC-MS power supply is performed. First, the coexistence of tiny and larger nanoparticles is demonstrated with the absorption spectra. Then, based on the Light Extinction Spectroscopy (LES) diagnostics, Ag NPs larger than 20 nm are captured and the PSDs are illustrated to be poly-disperse, which is also validated by the TEM results. The temporal particle growth is discussed in terms of the De Brouckere mean diameter. Even though the same sputtering energy is applied (*i.e.*, the same amount of silver atoms incorporated in silicone oil at the end of plasma treatment), the growth kinetics of Ag NPs in silicone oil differ due to the different deposition rates. In fact, particle aggregation is promoted at higher deposition rates due to the area of higher concentration at the plasma–liquid interface. Additionally, increased stirring yields the formation of smaller NPs but does not substantially affect the final size in our range of working conditions. As in the study of Deng *et al.* (Pt/Cu alloy NPs in PEG),[10] our LES results confirm that aggregation and growth of Ag NPs take place both at the interface and inside the silicone oil. The temporal variations in the absorption spectra and temporal increase in the particle size reveal low colloidal stability of Ag NPs in silicone oil. That is, silicone oil may not be a good capping agent for Ag NPs under our experimental conditions, but the introduction of additional stabilizing agents inside the host liquid before sputtering can help to obtain stable suspensions with smaller NPs.[66] Yet, prolonged experimentation is required to draw a conclusion.

In the short term, experiments at even lower deposition rates and different stirring speeds can be conducted to better track particle aggregation with the LES technique. Measurements at different levels of the cuvette can be carried out to check the gradient in the particle concentration. Prolonged waiting periods after the plasma treatment (under the same vacuum) can be studied, as well as the comparison of the air exposure in the ambient (during storage) prior to *ex situ* analyses. Further LES measurements can be acquired during the High-Power Impulse Magnetron Sputtering (HiPIMS) and bipolar HiPIMS (B-HiPIMS) methods. Compared to DC-MS, the sputtered metal atoms are ionized and possess higher kinetic energy (few tens of eV) in HiPIMS,[67] and these ions are further accelerated in B-HiPIMS with decent control over their energies.[68,69] The accelerated species dissipate their energy while penetrating through the liquid surface, causing local heat-up and reduction in the liquid viscosity. Therefore, higher kinetic energy levels influence the properties of the NPs due to the varied interactions at the plasma–liquid interface, which should be explored to fine-tune the NPs. This fine-tuning can even be carried out online during the deposition. The LES observations might help to better understand the NP formation process during reactive magnetron sputtering deposition.[70] Moreover, the LES technique can also be implemented into other nanofluid synthesis methods, such as electrode erosion using discharges in liquids,[71] evaporation in vacuum onto liquids,[72] sputtering-based Gas Aggregation cluster Source (GAS),[61] in a stopped-flow device during a chemical reduction.[52]

Despite their lure as an efficient heat transfer strategy,[73] nanofluids are still not in practice as the working fluid due to the inconsistent experimental results. The preparation of the nanofluids (two-step method or chemical synthesis) mostly includes miscellaneous stabilizers that can interact with the material of the heat-transfer device, yielding material loss.[74] Hence, the tribological effects of the nanofluids (corrosion, erosion, and abrasion), together with the particle stability, could be resolved by magnetron sputtering onto liquids. Thus, the LES technique can provide a robust basis for the *in situ* and real-time size characterization of mono- or poly-disperse, nano- to submicron particles in a plasma environment to fine-tune the particle size.

Author contributions

Conceptualization, S. K.; methodology, P. E., Y. T. A., and A. S.; software, P. E. and Y. T. A.; validation, P. U.; formal analysis, P. E. and Y. T. A.; investigation, A. S.; resources, S. K. and M. R. V.; data curation, P. E. and Y. T. A.; writing–original draft preparation, P. E., A. S., Y. T. A., P. U., S. K., and M. R. V.; writing–review and editing, P. E., A. S., Y. T. A., P. U., S. K., and M. R. V.; visualization, P. E. and Y. T. A.; supervision, S. K. and M. R. V.; project administration, S. K. and M. R. V.; funding acquisition, S. K. and M. R. V. All authors have read and agreed to the published version of the manuscript.

Conflicts of interest

There are no conflicts to declare.

Acknowledgements

P. E., Y. T. A., and M. R. V. acknowledge the Interne Fondsen KU Leuven/Internal Funds KU Leuven (C3/21/029). S. K. and A. S. thank the FNRS for the financial support through the "SOLUTIoN" project (No. T.0134.19). S. K. is a senior research associate of the National Fund for Scientific Research (FNRS, Belgium). The authors also acknowledge Prof. Michel Voue for the ellipsometry measurements.

References

1 S. U. Choi and J. A. Eastman, *ASME International Mechanical Engineering Congress and Exposition*, 1995.
2 L. M. Liz-Marzán, *Mater. Today*, 2004, **7**, 26–31.
3 R. Taylor, S. Coulombe, T. Otanicar, P. Phelan, A. Gunawan, W. Lv, G. Rosengarten, R. Prasher and H. Tyagi, *J. Appl. Phys.*, 2013, **113**, 011301.
4 J. Xu, M. Ramasamy, T. Tang, Y. Wang, W. Zhao and K. C. Tam, *J. Colloid Interface Sci.*, 2022, **623**, 883–896.
5 S. Zhang, W. Jiang, G. Liu, S. Liu, H. Chen, G. Lyu, G. Yang, Y. Liu and Y. Ni, *J. Colloid Interface Sci.*, 2023, **629**, 766–777.
6 A. Sergievskaya, A. Chauvin and S. Konstantinidis, *Beilstein J. Nanotechnol.*, 2022, **13**, 10–53.
7 T. B. Gorji and A. A. Ranjbar, *Renew. Sustain. Energy Rev.*, 2017, **72**, 10–32.
8 H. Wender, P. Migowski, A. F. Feil, S. R. Teixeira and J. Dupont, *Coord. Chem. Rev.*, 2013, **257**, 2468–2483.
9 A. Sergievskaya, A. O'Reilly, H. Alem, J. De Winter, D. Cornil, J. Cornil and S. Konstantinidis, *Front. Nanotechnol.*, 2021, **3**, 710612.
10 L. Deng, M. T. Nguyen, S. Mei, T. Tokunaga, M. Kudo, S. Matsumura and T. Yonezawa, *Langmuir*, 2019, **35**, 8418–8427.
11 A. Sergievskaya, A. O'Reilly, A. Chauvin, J. Veselý, A. Panepinto, J. De Winter, D. Cornil, J. Cornil and S. Konstantinidis, *Colloids Surf., A*, 2021, **615**, 126286.
12 D. Depla, *Magnetrons, Reactive Gases and Sputtering*, Diederik Depla, 2013.

13 K. Wasa, M. Kitabatake and H. Adachi, *Thin Film Materials Technology: Sputtering of Control Compound Materials*, Springer Science & Business Media, 2004.

14 Y. Hatakeyama, S. Takahashi and K. Nishikawa, *J. Phys. Chem. C*, 2010, **114**, 11098–11102.

15 Y. Hatakeyama, K. Onishi and K. Nishikawa, *RSC Adv.*, 2011, **1**, 1815–1821.

16 M. Meischein, X. Wang and A. Ludwig, *J. Phys. Chem. C*, 2021, **125**, 24229–24239.

17 Y. Ishida, R. Nakabayashi, M. Matsubara and T. Yonezawa, *New J. Chem.*, 2015, **39**, 4227–4230.

18 T. Sumi, S. Motono, Y. Ishida, N. Shirahata and T. Yonezawa, *Langmuir*, 2015, **31**, 4323–4329.

19 A. Chauvin, A. Sergievskaya, A. Fucikova, C. A. Corrêa, J. Vesely, J. Cornil, D. Cornil, M. Dopita and S. Konstantinidis, *Nanoscale Adv.*, 2021, **3**, 4780–4789.

20 T. Torimoto, K.-i. Okazaki, T. Kiyama, K. Hirahara, N. Tanaka and S. Kuwabata, *Appl. Phys. Lett.*, 2006, **89**, 243117.

21 A. Sergievskaya, R. Absil, A. Chauvin, K. V. Yusenko, J. Veselý, T. Godfroid and S. Konstantinidis, *Phys. Chem. Chem. Phys.*, 2023, 2803–2809.

22 J. A. Thornton, *Thin Solid Films*, 1978, **54**, 23–31.

23 A.-L. Thomann, A. Caillard, M. Raza, M. El Mokh, P. Cormier and S. Konstantinidis, *Surf. Coat. Technol.*, 2019, **377**, 124887.

24 V. Orozco-Montes, A. Caillard, P. Brault, W. Chamorro-Coral, J. Bigarre, A. Sauldubois, P. Andreazza, S. Cuynet, S. Baranton and C. Coutanceau, *J. Phys. Chem. C*, 2021, **125**, 3169–3179.

25 K. Patel, A. Sergievskaya, S. Chauhan and S. Konstantinidis, *J. Appl. Phys.*, 2022, **131**, 203301.

26 Y. Hatakeyama, T. Morita, S. Takahashi, K. Onishi and K. Nishikawa, *J. Phys. Chem. C*, 2011, **115**, 3279–3285.

27 M. M. D. Luna and M. Gupta, *Appl. Phys. Lett.*, 2018, **112**, 201605.

28 Y. Ishida, S. Udagawa and T. Yonezawa, *Colloids Surf., A*, 2016, **498**, 106–111.

29 E. Vanecht, K. Binnemans, J. W. Seo, L. Stappers and J. Fransaer, *Phys. Chem. Chem. Phys.*, 2011, **13**, 13565–13571.

30 E. F. Borra, O. Seddiki, R. Angel, D. Eisenstein, P. Hickson, K. R. Seddon and S. P. Worden, *Nature*, 2007, **447**, 979–981.

31 H. Wender, L. F. de Oliveira, A. F. Feil, E. Lissner, P. Migowski, M. R. Meneghetti, S. R. Teixeira and J. Dupont, *Chem. Commun.*, 2010, **46**, 7019–7021.

32 H. Wender, R. V. Gonçalves, A. F. Feil, P. Migowski, F. S. Poletto, A. R. Pohlmann, J. Dupont and S. R. Teixeira, *J. Phys. Chem. C*, 2011, **115**, 16362–16367.

33 A. Rezníčková, P. Slepicka, N. Slavikova, M. Staszek and V. Svorcik, *Colloids Surf., A*, 2017, **523**, 91–97.

34 P. Slepička, R. Elashnikov, P. Ulbrich, M. Staszek, Z. Kolská and V. Švorčík, *J. Nanoparticle Res.*, 2015, **17**, 11.

35 F. Onofri, M. Wozniak and S. Barbosa, *Contrib. Plasma Phys.*, 2011, **51**, 228–236.

36 G. Crawley, M. Cournil and D. D. Benedetto, *Powder Technol.*, 1997, **91**, 197–208.

37 R. Xu, *Particle Characterization: Light Scattering Methods*, Kluwer Academic Publishers, Miami, 2002.

38 G. Mie, *Ann. Phys.*, 1908, **330**, 377–445.

39 J. M. Smith, A. Roth, D. E. Huffman, Y. M. Serebrennikova, J. Lindon and L. H. García-Rubio, *Appl. Spectrosc.*, 2012, **66**, 1186–1196.

40 S. Barbosa, F. R. A. Onofri, L. Couëdel, M. Wozniak, C. Montet, C. Pelcé, C. Arnas, L. Boufendi, E. Kovacevic, J. Berndt, *et al.*, *J. Plasma Phys.*, 2016, **82**, 615820403.

41 H. Horvath and C. Dellago, *J. Aerosol Sci.*, 1993, **24**, 143–154.

42 P. Eneren, Y. T. Aksoy, Y. Zhu, E. Koos and M. R. Vetrano, *J. Quant. Spectrosc. Radiat. Transf.*, 2021, **261**, 107494.

43 P. Eneren, PhD thesis, KU Leuven, Belgium, 2022.

44 H. Kersten, H. Deutsch, H. Steffen, G. Kroesen and R. Hippler, *Vacuum*, 2001, **63**, 385–431.

45 S. Panigrahi, S. Praharaj, S. Basu, S. K. Ghosh, S. Jana, S. Pande, T. Vo-Dinh, H. Jiang and T. Pal, *J. Phys. Chem. B*, 2006, **110**, 13436–13444.

46 C.-N. Lok, C.-M. Ho, R. Chen, Q.-Y. He, W.-Y. Yu, H. Sun, P. K.-H. Tam, J.-F. Chiu and C.-M. Che, *JBIC, J. Biol. Inorg. Chem.*, 2007, **12**, 527–534.

47 Y. A. Krutyakov, A. A. Kudrinskiy, A. Y. Olenin and G. V. Lisichkin, *Russ. Chem. Rev.*, 2008, **77**, 233.

48 I. Pastoriza-Santos and L. M. Liz-Marzán, *J. Mater. Chem.*, 2008, **18**, 1724–1737.

49 C. F. Bohren and D. R. Huffman, in *Absorption and Scattering of Light by Small Particles*, Wiley, New York, 1983, ch. 4.3, pp. 100–101.

50 T. Kourti, in *Turbidimetry in Particle Size Analysis*, American Cancer Society, 2006, ch. 6.2, p. 21.

51 W. S. M. Werner, K. Glantschnig and C. Ambrosch-Draxl, *J. Phys. Chem. Ref. Data*, 2009, **38**, 1013–1092.

52 B. Abécassis, F. Testard, O. Spalla and P. Barboux, *Nano Lett.*, 2007, **7**, 1723–1727.

53 V. V. Tatarchuk, A. P. Sergievskaya, T. M. Korda, I. A. Druzhinina and V. I. Zaikovsky, *Chem. Mater.*, 2013, **25**, 3570–3579.

54 E. Vanecht, K. Binnemans, S. Patskovsky, M. Meunier, J. W. Seo, L. Stappers and J. Fransaer, *Phys. Chem. Chem. Phys.*, 2012, **14**, 5662–5671.

55 R. D. Corpuz, Y. Ishida and T. Yonezawa, *New J. Chem.*, 2017, **41**, 6828–6833.

56 S. Barbosa, L. Couëdel, C. Arnas, K. K. Kumar, C. Pardanaud and F. R. A. Onofri, *J. Phys. D: Appl. Phys.*, 2015, **49**, 045203.

57 H. Wender, P. Migowski, A. F. Feil, L. F. de Oliveira, M. H. G. Prechtl, R. Leal, G. Machado, S. R. Teixeira and J. Dupont, *Phys. Chem. Chem. Phys.*, 2011, **13**, 13552–13557.

58 J. Drewes, S. Rehders, T. Strunskus, H. Kersten, F. Faupel and A. Vahl, *Part. Part. Syst. Char.*, 2022, **39**, 2200112.

59 E. Redel, M. Walter, R. Thomann, L. Hussein, M. Krüger and C. Janiak, *Chem. Commun.*, 2010, **46**, 1159–1161.

60 M. Wagener, B. S. Murty and B. Günther, *MRS Online Proc. Libr.*, 1996, **457**, 149–154.

61 K. Biliak, D. Nikitin, S. Ali-Ogly, M. Protsak, P. Pleskunov, M. Tosca, A. Sergievskaya, D. Cornil, J. Cornil, S. Konstantinidis, T. Košutová, Z. Černochová, P. Štěpánek,

J. Hanuš, J. Kousal, L. Hanyková, I. Krakovský and A. Choukourov, *Nanoscale Adv.*, 2023, **5**, 955–969.

62 S. C. Hamm, S. Basuray, S. Mukherjee, S. Sengupta, J. C. Mathai, G. A. Baker and S. Gangopadhyay, *J. Mater. Chem. A*, 2014, **2**, 792–803.

63 Y. Ishida, S. Udagawa and T. Yonezawa, *Colloids Surf., A*, 2016, **504**, 437–441.

64 Y. Hatakeyama, M. Okamoto, T. Torimoto, S. Kuwabata and K. Nishikawa, *J. Phys. Chem. C*, 2009, **113**, 3917–3922.

65 Y. Ishida, I. Akita, T. Sumi, M. Matsubara and T. Yonezawa, *Sci. Rep.*, 2016, **6**, 29928.

66 Y. Ishida, R. Nakabayashi, R. D. Corpuz and T. Yonezawa, *Colloids Surf., A*, 2017, **518**, 25–29.

67 K. Sarakinos, J. Alami and S. Konstantinidis, *Surf. Coat. Technol.*, 2010, **204**, 1661–1684.

68 N. Britun, M. Michiels, T. Godfroid and R. Snyders, *Appl. Phys. Lett.*, 2018, **112**, 234103.

69 J. Keraudy, R. P. B. Viloan, M. A. Raadu, N. Brenning, D. Lundin and U. Helmersson, *Surf. Coat. Technol.*, 2019, **359**, 433–437.

70 S. Ibrahim, V. Ntomprougkidis, M. Goutte, G. Monier, M. Traïkia, J.-M. Andanson, P. Bonnet and A. Bousquet, *Nanoscale*, 2023, **15**, 5499–5509.

71 A. V. Nominé, T. Gries, C. Noel, A. Nominé, V. Milichko and T. Belmonte, *J. Appl. Phys.*, 2021, **130**, 151101.

72 A. Fujita, Y. Matsumoto, M. Takeuchi, H. Ryuto and G. H. Takaoka, *Phys. Chem. Chem. Phys.*, 2016, **18**, 5464–5470.

73 Y. T. Aksoy, Y. Zhu, P. Eneren, E. Koos and M. R. Vetrano, *Energies*, 2021, **14**, 80.

74 P. Eneren, Y. T. Aksoy and M. R. Vetrano, *Energies*, 2022, **15**, 2525.